INVERSE HOMOGENIZATION AND DESIGN OF MICROSTRUCTURE FOR POINTWISE STRESS CONTROL

by R. LIPTON[†] *and* M. STUEBNER

(*Mathematics Department, Louisiana State University, Baton Rouge*, LA 70803, *USA*)

Summary

New higher-order homogenization results are employed in an inverse homogenization procedure to identify graded microstructures that provide desirable structural response while ensuring stress control near joints or junctions between structural elements. The methodology is illustrated for long cylindrical shafts reinforced with stiff cylindrical elastic fibres with generators parallel to the shaft. The local fibre geometry can change across the shaft cross-section. The methodology is implemented numerically for cross-sectional shapes that possesses reentrant corners typically seen in lap joints and junctions of struts. Graded locally layered microgeometries are identified that provide the required structural rigidity with respect to torsion loading while at the same time mitigating the influence of stress concentrations at the reentrant corners.

1. Introduction

Modern design practice increasingly incorporates the use of load bearing components made from composite materials. Composites are now used in structural geometries that involve abrupt dimensional changes within structural components, such as skins connected to ribs, panel reinforcements and junctions of struts. Associated with these geometries are stress concentrations and the potential for failure. In this paper a design strategy is formulated for identifying graded microstructures that can be used to control the local fluctuating stresses near stress concentrations induced by rivets, bolts or reentrant corners. Reentrant corners are typically found in lap joints and near the junction between stiffeners and panels.

The inverse homogenization design method is based upon the formulation of a homogenized design problem expressed in terms of suitable macroscopic quantities that satisfy two requirements. The first is that the homogenized design problem should be computationally tractable. The second requirement is that the solution of the homogenized design problem must provide the means to explicitly identify graded microstructures that engender suitable structural response while at the same time control local fluctuating stresses in regions located near stress concentrations.

It is now well known that effective macroscopic constitutive properties relating average stress to average strain can be employed in the numerical design of composite structures for optimal structural compliance and natural frequency. This type of design problem has received significant attention from both the applied mathematics and structural optimization communities in the 1980s

---

[†] ⟨lipton@math.lsu.edu⟩

and 1990s; see for example (**1** to **10**). This list is by no means complete and for a description of the history of the problem and extensive references to the literature the reader is referred to (**11** to **18**). In the context of functionally graded materials this design strategy for optimizing structural properties appears in (**19**, **20**). In all of these works the problem of determining the optimal spatial dependence for the composition is obtained through the use of effective macroscopic constitutive relations.

Recent efforts have initiated the development of numerical methods for structural optimization in the presence of stress constraints. The investigation given in (**21**) provides a numerical method for the stress constrained minimum volume design problem. The method is carried out using an empirical model that is an extension of the power penalized stiffness model also known as the solid isotropic microstructure with penalization (SIMP) model (**18**). The choice of local stress constraints proposed in (**21**) is motivated by the explicit form of the corrector tensors associated with rank-two orthogonal laminar microstructures. The problem of design of long fibre reinforced shafts for maximum torsional rigidity in the presence of mean square stress constraints is addressed in (**22**). A rigorous inverse homogenization method for the optimal distribution of fibre diameters across the shaft is developed. It is shown that the appropriate homogenized problem requires the use of the second moment or covariance tensor in addition to the effective compliance. This methodology can be applied to the design of graded locally periodic microstructures involving multiple anisotropic phases in three dimensional elastic structures (**23**). Very recently (**24**) a homogenization method for topology design subject to mean square stress constraints using locally layered microstructures of arbitrary rank has been developed.

For problems of thermal conduction the work of (**25**) considers the problem of finding microstructures that minimize the mean square deviation of the temperature gradient from a prescribed target. The analysis given in (**25**) provides the connection between minimizing sequences of optimal locally layered microstructures and the optimal design coming from the homogenized problem. This connection is shown to apply for an implicitly defined set of target fields. For composites made of two isotropic phases the work of (**26**, **27**) shows that minimizing sequences of discrete microstructures can be found within the class of locally layered materials for any choice of target field. The work of (**28**) provides an explicit formula for the homogenized optimization problem and characterizes all possible minimizing sequences of microstructures. This is used to rule out the appearance of minimizing sequences of layered configurations with more than one scale of oscillation. Another recent development is given in (**29**). Here for any choice of target the notion of constrained quasiconvexity is applied and is used to identify minimizing sequences of locally layered microstructures. We close by pointing out that methods developed in (**30**) for non-self adjoint optimization problems may be applied to the problems of optimal design subject to mean square stress constraints.

In all of the aforementioned work the stress constraints or objective functions were of mean square type. In this work a rigorous design methodology is presented that allows for tighter control of local stresses at the level of the microstructure. This is important when designing against failure initiation. In what follows we provide a new methodology that delivers graded materials that provide pointwise control of the stress inside subdomains with boundaries that do not intersect the boundary of the structure. In order to proceed new macroscopic properties beyond effective constitutive laws and covariance tensors are required. In this work we make use of the macrofield modulation functions and the homogenization constraints given in (**31** to **33**). The macrofield modulation functions together with effective constitutive relations are used here to construct a suitable homogenized design problem that satisfies the two requirements associated with the inverse homogenization design method.

To illustrate the ideas this article treats the problem of reinforcement of a long shaft with constant cross-section subjected to torsion loading. The microstructure within the shaft consists of long reinforcement fibres of constant cross-section with isotropic shear modulus G_2 embedded in a more compliant material with shear modulus G_1. The shaft together with the fibres are right cylinders with generators along the x_3-axis and the cross-section of the reinforced shaft is constant and specified by a region Ω in the (x_1, x_2)-plane. The characteristic length scale of the microgeometry is assumed to be small relative to the dimensions of the shaft cross-section and is denoted by ε. In the neighbourhood of any point $\mathbf{x} = (x_1, x_2)$ the local microgeometry is given by layers of stiff material interspersed with layers of compliant material. The thicknesses of the stiff and compliant layers are specified by $\varepsilon\theta_2$ and $\varepsilon\theta_1$ respectively, with $\theta_1 + \theta_2 = 1$. The layer normals are specified by the angle γ. The thickness of the layers and layering orientation is free to change across the cross-section; see Fig. 1. For future reference this type of microstructure is called a locally layered microstructure.

In what follows a constraint is placed on the total cross-sectional area occupied by the stiff material. The goal of the design problem is to identify a distribution of local layer orientations and relative layer thicknesses across the cross-section such that the following requirements are met.

(i) The reinforced shaft has a torsional rigidity that is acceptable.
(ii) The magnitude of the local stress at the length scale of the microstructure is controlled over a designated subset of the cross-section.

In section 2 we present the homogenized problem and describe the inverse homogenization method for identifying suitable locally layered designs satisfying requirements (i) and (ii). The theoretical results presented here can be applied to fully three-dimensional problems using locally layered microstructures; this issue is taken up in the Conclusion. It is pointed out that the inverse homogenization design method for graded locally periodic microstructures is rigorously established in the context of multi-phase three-dimensional elasticity in (23). In section 3 the numerical implementation for the inverse homogenization design method is discussed. The inverse homogenization design method is carried out for X-shaped and L-shaped shaft cross-sections; see section 4.
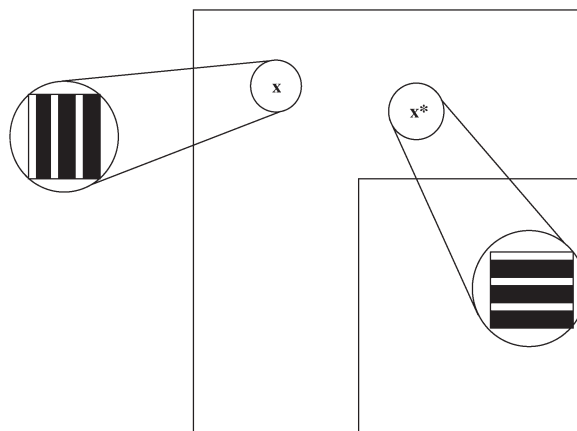

Fig. 1 Domain filled with a graded locally layered microstructure. The local layer orientations in the neighbourhood of the points $\mathbf{x}$ and $\mathbf{x}^*$ are displayed

These geometries typify the junctions between composite substructures and possesses reentrant corners typically seen in lap joints and junctions of struts. Sections 5 and 6 develop the theory behind the inverse homogenization method for pointwise stress control.

It is clear that the theoretical and numerical treatment presented here falls short of addressing many of the issues pertinent to the design of actual bonded composite structures. However, the approach given introduces the appropriate physical quantities within a mathematically rigorous context and uses these to construct a numerically feasible strategy for the design of microstructures within structural elements.

2. Inverse homogenization method

In this section we state the homogenized design problem and provide the explicit connection between the optimal homogenized design and a desirable locally layered microgeometry that satisfies pointwise stress constraints while delivering a torsional rigidity close to that of the optimal homogenized design.

The design variables for the homogenized design problem are given by the local relative layer thickness of material one, θ_1, and the layer angle γ. The relative layer thickness of material two is denoted by θ_2 and $\theta_1 + \theta_2 = 1$. These design variables can change across the shaft cross-section and are functions of $\mathbf{x}$. The associated vector of design variables is denoted by $\mathcal{B}$ and $\mathcal{B}(\mathbf{x}) = (\theta_1(\mathbf{x}), \gamma(\mathbf{x}))$. The resource constraint on the amount of stiff material that can be used to reinforce the shaft cross-section is given by

$$\int_\Omega (1 - \theta_1(\mathbf{x})) \, dx_1 \, dx_2 \leqslant \Theta \times (\text{Area of } \Omega), \tag{2.1}$$

where $0 < \Theta < 1$. At each point the design vector satisfies the box constraints given by

$$0 < \theta_1^{\min} \leqslant \theta_1 \leqslant \theta_1^{\max} < 1 \quad \text{and} \quad 0 \leqslant \gamma \leqslant 2\pi. \tag{2.2}$$

Here the constraints on the relative layer thickness θ_1 correspond to microstructured material filling out the entire design domain. The local microgeometry specified by $\mathcal{B}$ changes continuously with position and

$$|\theta_1(\mathbf{x}) - \theta_1(\mathbf{x} + \mathbf{h})| \leqslant K|\mathbf{h}|^\alpha, \qquad |\gamma(\mathbf{x}) - \gamma(\mathbf{x} + \mathbf{h})| \leqslant K|\mathbf{h}|^\alpha \tag{2.3}$$

for fixed constants K and α such that $0 < \alpha \leqslant 1$. The set of all design vectors $\mathcal{B}$ satisfying the resource constraint, box constraints, and (2.3) is denoted by D_Θ.

The compliance in shear for each material is given by $S_1 = (2G_1)^{-1}$ and $S_2 = (2G_2)^{-1}$. Here material one is assumed to be the more compliant material, $S_1 > S_2$. The effective compliance tensor $S^E(\mathcal{B})$ is given by

$$S^E(\mathcal{B}(\mathbf{x})) = R(\gamma(\mathbf{x}))D(\theta_1(\mathbf{x}))R^T(\gamma(\mathbf{x})), \tag{2.4}$$

where $R(\gamma)$ is the matrix associated with an anti-clockwise rotation of γ radians and

$$D(\theta_1) = \begin{bmatrix} (\theta_1 S_1^{-1} + (1 - \theta_1)S_2^{-1})^{-1} & 0 \\ 0 & \theta_1 S_1 + (1 - \theta_1)S_2 \end{bmatrix}. \tag{2.5}$$

The macroscopic stress potential ϕ^H vanishes on the boundary of the cross-section and satisfies

$$-\operatorname{div}\left(S^E(\mathcal{B})\nabla\phi^H\right) = 1 \tag{2.6}$$

inside the cross-section. The torsional rigidity for the homogenized shaft cross-section made from a homogenized material with compliance $S^E(\mathcal{B})$ is given by

$$\mathcal{R}(\mathcal{B}) = 2\int_{\Omega} \phi^H \, dx_1 \, dx_2. \tag{2.7}$$

The stress in the homogenized shaft is given by $\sigma^H = R\nabla\phi^H$, where R is the rotation matrix associated with an anti-clockwise rotation of $\pi/2$ radians.

The macroscopic stress constraints associated with materials one and two are given in terms of the macrostress modulation functions introduced in (**31**). We define the matrices

$$Q_1(\mathcal{B}(\mathbf{x})) = R(\gamma(\mathbf{x}))(\Lambda_1(\theta_1(\mathbf{x})))^2 R^T(\gamma(\mathbf{x})), \tag{2.8}$$

$$Q_2(\mathcal{B}(\mathbf{x})) = R(\gamma(\mathbf{x}))(\Lambda_2(\theta_1(\mathbf{x})))^2 R^T(\gamma(\mathbf{x})), \tag{2.9}$$

where the 2×2 matrices $\Lambda_1(\theta_1)$ and $\Lambda_2(\theta_1)$ are given by

$$\Lambda_1(\theta_1) = \begin{bmatrix} 1 - \dfrac{(S_2 - S_1)(1 - \theta_1)}{\theta_1 S_1 + (1 - \theta_1)S_2} & 0 \\ 0 & 1 \end{bmatrix} \quad \text{and} \quad \Lambda_2(\theta_1) = \begin{bmatrix} 1 + \dfrac{(S_2 - S_1)\theta_1}{(\theta_1 S_1 + (1 - \theta_1)S_2} & 0 \\ 0 & 1 \end{bmatrix}.$$

The explicit formulae for the macrostress modulations are given by

$$f_1(\mathcal{B}(\mathbf{x}), \mathbf{v}) = Q_1(\mathcal{B}(\mathbf{x}))\mathbf{v} \cdot \mathbf{v} \quad \text{if } \theta_1(\mathbf{x}) > 0, \quad f_1(\mathcal{B}(\mathbf{x}), \mathbf{v}) = 0 \quad \text{if } \theta_1 = 0, \tag{2.10}$$

$$f_2(\mathcal{B}(\mathbf{x}), \mathbf{v}) = Q_2(\mathcal{B}(\mathbf{x}))\mathbf{v} \cdot \mathbf{v} \quad \text{if } \theta_2(\mathbf{x}) > 0, \quad f_2(\mathcal{B}(\mathbf{x}), \mathbf{v}) = 0 \quad \text{if } \theta_2 = 0 \tag{2.11}$$

for every vector $\mathbf{v}$. We choose a subset $\mathcal{S}$ of the shaft cross-section that lies a finite distance away from the boundary. On this set the prescribed macroscopic stress constraints are

$$f_1(\mathcal{B}(\mathbf{x}), \nabla\phi^H(\mathbf{x})) \leqslant T^2, \quad f_2(\mathcal{B}(\mathbf{x}), \nabla\phi^H(\mathbf{x})) \leqslant T^2. \tag{2.12}$$

In this treatment domains with reentrant corners are considered and so there will be a stress singularity at each such corner. Therefore the choice of $T > 0$ depends on the distance between $\mathcal{S}$ and the reentrant corner. It is clear that the stress constraint might not be satisfied by any homogenized design if T is chosen too small.

The homogenized design problem is given by

$$HP = \left\{ \inf\{\mathcal{R}(\mathcal{B})\} \, ; \text{ subject to: } \begin{cases} \mathcal{B} \text{ in } D_\Theta, \\ f_i(\mathcal{B}(\mathbf{x}), \nabla\phi^H(\mathbf{x})) \leqslant T^2, \, i = 1, 2 \quad \text{for } \mathbf{x} \text{ in } \mathcal{S}. \end{cases} \right\}$$

In what follows it is supposed that at least one design $\mathcal{B}$ in D_Θ satisfies (2.12).

THEOREM 2.1. *There is a design vector $\hat{\mathcal{B}}$ in D_Θ for which the infimum of the homogenized design problem HP is attained.*

This is demonstrated in section 5.

Next we present the class of locally layered microstructures for which a microstructure satisfying the requirements (i) and (ii) can be identified using the information given by the optimal design $\hat{\mathcal{B}}$ of the homogenized design problem.

Consider a partition of the shaft cross-section into the N subdomains ω^k, $k = 1, \ldots, N$, such that $\overline{\Omega} = \bigcup_k^N \overline{\omega}^k$. Here the maximum diameter of the subdomains in the partition is denoted by τ^N. We denote such a partition by $\mathcal{P}_{\tau^N}$. Inside the kth subdomain the stiff material is given by layers of thickness $\varepsilon \theta_2^k$ separated by layers of compliant material of thickness $\varepsilon \theta_1^k$, with $\theta_1^k + \theta_2^k = 1$. The layer normals inside ω^k are specified by the angle γ^k and are given by $\mathbf{n}^k = (\cos \gamma^k, \sin \gamma^k)$. As before θ_1^k and γ^k satisfy the box constraints

$$0 \leqslant \theta_1^{\min} \leqslant \theta_1^k \leqslant \theta_1^{\max} < 1, \quad 0 \leqslant \gamma^k \leqslant 2\pi, \quad k = 1, \ldots, N. \tag{2.13}$$

The characteristic function of the set occupied by material one for such a layered microgeometry is denoted by $\chi_1^{\varepsilon,N}$, where $\chi_1^{\varepsilon,N} = 1$ inside material one and zero outside and $\chi_2^{\varepsilon,N} = 1 - \chi_1^{\varepsilon,N}$. The rapidly oscillating piecewise constant compliance for such a layered microgeometry is denoted by $S^{\varepsilon,N}$ and $S^{\varepsilon,N} = S_1 \chi_1^{\varepsilon,N} + S_2 \chi_2^{\varepsilon,N}$.

The stress potential associated with a locally layered microgeometry is denoted by $\phi^{\varepsilon,N}$ and vanishes on the boundary of the cross-section. The stress potential satisfies the equilibrium equation

$$- \operatorname{div} \left(S^{\varepsilon,N} \nabla \phi^{\varepsilon,N} \right) = 1. \tag{2.14}$$

The torsional rigidity of the cross-section is given by

$$\mathcal{R}^{\varepsilon,N} = 2 \int_{\Omega} \phi^{\varepsilon,N} \, dx_1 \, dx_2. \tag{2.15}$$

Lastly we recall that the non-zero components of the in plane stress denoted by the vector $\sigma^{\varepsilon,N} = (\sigma_{13}^{\varepsilon,N}, \sigma_{23}^{\varepsilon,N})$ are related to the gradient of the stress potential according to

$$\sigma^{\varepsilon,N} = R \nabla \phi^{\epsilon,N}, \tag{2.16}$$

where the matrix R corresponds to an anti-clockwise rotation of $\pi/2$ and $|\sigma^{\varepsilon,N}| = |\nabla \phi^{\varepsilon,N}|$.

For a given tolerance T the ultimate goal would be to identify a locally layered microstructure specified by $S^{\varepsilon,N}$ with an acceptable torsional rigidity and stress potential satisfying the stress constraints in each of the materials over the prescribed set $\mathcal{S}$ given by

$$\chi_1^{\varepsilon,N}(\mathbf{x})|\nabla \phi^{\varepsilon,N}(\mathbf{x})| \leqslant T \quad \text{and} \quad \chi_2^{\varepsilon,N}(\mathbf{x})|\nabla \phi^{\epsilon,N}(\mathbf{x})| \leqslant T. \tag{2.17}$$

In what follows we show that it is possible to enforce these stress constraints in a controlled asymptotic fashion and simultaneously construct a locally layered microstructure with torsional rigidity close to $\mathcal{R}(\hat{\mathcal{B}})$.

THEOREM 2.2 (Identification of graded microstructure). *For any given $t > T$ and small number $\delta > 0$, one can construct a partition $\mathcal{P}_{\tau^{N_0}}$ and locally layered microstructure specified by S^{ε_0,N_0} for which the part of $\mathcal{S}$ over which the constraints*

$$\chi_1^{\varepsilon_0,N_0}(\mathbf{x})|\nabla \phi^{\varepsilon_0,N_0}(\mathbf{x})| \leqslant t \quad \text{and} \quad \chi_2^{\varepsilon_0,N_0}(\mathbf{x})|\nabla \phi^{\epsilon_0,N_0}(\mathbf{x})| \leqslant t \tag{2.18}$$

are violated has measure (area) less than δ and

$$|\mathcal{R}^{\varepsilon_0,N_0} - \mathcal{R}(\hat{\mathcal{B}})| < \delta, \tag{2.19}$$

and

$$\int_{\Omega} (1 - \chi_1^{\varepsilon_0,N_0}) \, dx_1 dx_2 \leqslant \Theta \times (\text{Area of } \Omega) + \delta. \tag{2.20}$$

Inside each subdomain ω^k associated with the partition $\mathcal{P}_{\tau N_0}$ the local layer directions and area fractions are determined from the optimal homogenized design $\hat{\mathcal{B}} = (\hat{\theta}_1, \hat{\gamma})$ through the averages given by

$$\hat{\theta}_1^k = \frac{1}{\text{Area of } \omega^k} \int_{\omega^k} \hat{\theta}_1(\mathbf{x}) \, dx_1 \, dx_2, \quad \hat{\gamma}^k = \frac{1}{\text{Area of } \omega^k} \int_{\omega^k} \hat{\gamma}(\mathbf{x}) \, dx_1 \, dx_2. \tag{2.21}$$

The systematic way in which the partition $\mathcal{P}_{\tau N_0}$ is chosen is provided in Remark 6.3 of section 6. Taken together, Theorems 2.1 and 2.2 provide an inverse homogenization method for identifying locally layered microstructures that satisfy pointwise stress constraints while delivering a torsional rigidity close to that given by the optimal design $\hat{\mathcal{B}}$ for the homogenized design problem.

3. Computational approach to the homogenized design problem

In the computational examples we enforce the stress constraint by adding a penalty term to the torsional rigidity and minimize

$$L = -\mathcal{R}(\mathcal{B}) + l \int_{\Omega} (f_i(\mathcal{B}(x), \nabla \phi^H))^p \, dx, \ i = 1, 2, \tag{3.1}$$

over all design vectors $\mathcal{B}$ in D_{Θ}, where $l > 0$ and ϕ^H satisfies

$$-\text{div}\left(S^E(\mathcal{B}) \nabla \phi^H\right) = 1 \tag{3.2}$$

and vanishes at the boundary. The computational examples provided here will be carried out for a domain with reentrant corners of interior angle $3\pi/2$. In view of the strength of the associated singularity at the reentrant corners the power p appearing in the penalty term is chosen to be less than 3. The existence of a minimizing design $\hat{\mathcal{B}}$ for this problem is guaranteed by the following theorem.

THEOREM 3.1. *There exists a design vector $\hat{\mathcal{B}}$ in D_{Θ} for which the infimum of (3.1) is obtained.*

This theorem is established in section 5.

As before we use the information given in the optimal design $\hat{\mathcal{B}}$ of (3.1) to construct a locally layered microstructure for which we have control of the pointwise stresses and for which the torsional rigidity is close to that of the optimal design for (3.1). This is formalized in the following theorem.

THEOREM 3.2 (Identification). *Given the optimal design $\hat{\mathcal{B}} = (\hat{\theta}_1, \hat{\gamma})$ for (3.1) with associated stress potential denoted by $\hat{\phi}^H$, consider the sets*

$$A_i^T = \{\mathbf{x} \text{ in } \Omega \text{ for which } f_i(\hat{\mathcal{B}}(x), \nabla \hat{\phi}^H) \leqslant T^2\}. \tag{3.3}$$

For a prescribed tolerance $\delta > 0$ and $t > T$ one can construct a partition $\mathcal{P}_{\tau N_0}$ and locally layered microstructure specified by S^{ε_0, N_0} for which the part of A_i^T over which the constraints

$$\chi_1^{\varepsilon_0, N_0}(\mathbf{x}) |\nabla \phi^{\varepsilon_0, N_0}(\mathbf{x})| \leqslant t \quad \text{and} \quad \chi_2^{\varepsilon_0, N_0}(\mathbf{x}) |\nabla \phi^{\epsilon_0, N_0}(\mathbf{x})| \leqslant t \tag{3.4}$$

are violated has measure (area) less than δ and

$$|\mathcal{R}^{\varepsilon_0, N_0} - \mathcal{R}(\hat{\mathcal{B}})| < \delta, \tag{3.5}$$

and

$$\int_{\Omega} (1 - \chi_1^{\varepsilon_0, N_0}) \, dx_1 \, dx_2 \leqslant \Theta \times (\text{Area of } \Omega) + \delta. \tag{3.6}$$

Inside each subdomain ω^k associated with the partition $\mathcal{P}_{\tau N_0}$ the local layer directions and area fractions are determined from the optimal homogenized design $\hat{\mathcal{B}} = (\hat{\theta}_1, \hat{\gamma})$ through the averages given by (2.21).

It is noted that this theorem follows from the same arguments used to justify Theorem 2.2.

The macrostress modulation functions (2.10) and (2.11) are discontinuous at $\theta_i = 0$. This is consistent with the fact that the stress amplification due to the presence of a second phase can persist even though only an infinitesimal amount of it is present. Since the objective function is differentiable on $0 < \theta_1^{\min} \leqslant \theta_1 \leqslant \theta_1^{\max} < 1$ the augmented objective function defined by (3.1) is optimized using a straightforward gradient minimization algorithm. For our computations we choose $\theta_1^{\min} = 0 \cdot 01$ and $\theta_1^{\max} = 0 \cdot 99$. To compute sensitivities we introduce the adjoint field λ. Here λ is the solution of

$$-\operatorname{div}\left(S^E(\mathcal{B})\nabla\lambda\right) = 1 + l\operatorname{div}\left(2p(Q_i(\mathcal{B})\nabla\phi^H \cdot \nabla\phi^H)^{p-1}Q_i(\mathcal{B})\nabla\phi^H\right), \qquad (3.7)$$

where $1 \leqslant p < 3$ and $\lambda = 0$ on the boundary. For $\eta \ll 1$ the change in ϕ^H due to small local perturbations $\eta\tilde{\theta}_1$, $\eta\tilde{\gamma}$ in the thickness and direction of the layers is written as $\tilde{\phi}$ and

$$-\operatorname{div}\left(S^E(\mathcal{B})\nabla\tilde{\phi}\right) = \operatorname{div}\left((\partial_{\theta_1}S^E(\mathcal{B})\tilde{\theta}_1 + \partial_\gamma S^E(\mathcal{B})\tilde{\gamma})\nabla\phi^H\right), \qquad (3.8)$$

where $\tilde{\phi} = 0$ on the boundary. The first variation with respect to the design variables θ_1 and γ gives to lowest order

$$\Delta L = -\int_\Omega \tilde{\phi}\,dx + \int_\Omega p(Q_i(\mathcal{B})\nabla\phi^H \cdot \nabla\phi^H)^{p-1}(\partial_{\theta_1}Q_i(\mathcal{B})\,\tilde{\theta} + \partial_\gamma Q_i(\mathcal{B})\,\tilde{\gamma})\nabla\phi^H \cdot \nabla\phi^H\,dx$$

$$+ \int_\Omega 2p(Q_i(\mathcal{B})\nabla\phi^H \cdot \nabla\phi^H)^{p-1}Q_i(\mathcal{B})\nabla\phi^H \cdot \nabla\tilde{\phi}\,dx. \qquad (3.9)$$

The choice of $\tilde{\theta}_1$ and $\tilde{\gamma}$ that renders ΔL the most negative is given by

$$\tilde{\theta}_1 = -\partial_{\theta_1}S^E(\mathcal{B})\nabla\lambda\nabla\phi^H - 2lp(Q_i(\mathcal{B})\nabla\phi^H \cdot \nabla\phi^H)^{p-1}\partial_{\theta_1}Q_i(\mathcal{B})\nabla\phi^H \cdot \nabla\phi^H, \qquad (3.10)$$

$$\tilde{\gamma} = -\partial_\gamma S^E(\mathcal{B})\nabla\lambda\nabla\phi^H - 2lp(Q_i(\mathcal{B})\nabla\phi^H \cdot \nabla\phi^H)^{p-1}\partial_\gamma Q_i(\mathcal{B})\nabla\phi^H \cdot \nabla\phi^H. \qquad (3.11)$$

The continuity constraints on $\theta_1(\mathbf{x})$, $\gamma(\mathbf{x})$ expressed by (2.3) are enforced by the way in which the design variables are initialized and updated. The local average of a scalar function f over the disk of radius R centred at $\mathbf{p}$ is denoted by $\langle f \rangle^R(\mathbf{p})$. For given fields θ_1, γ satisfying the resource and box constraints (2.1) and (2.2) the initial choice of design variables θ_1^0, γ^0 is given by

$$\theta_1^0 = \langle \theta_1 \rangle^R(\mathbf{x}) \quad \text{and} \quad \gamma^0 = \langle \gamma \rangle^R(\mathbf{x}). \qquad (3.12)$$

At the nth step we suppose that θ_1 and γ are given and we solve for ϕ and λ using the system of equations (3.2) and (3.7). Then θ_1 and γ are updated according to

$$\theta_{1,\text{new}} = \langle \theta_1 + \eta\tilde{\theta}_1 \rangle^R(\mathbf{x}) \quad \text{and} \quad \gamma_{\text{new}} = \langle \gamma + \eta\tilde{\gamma} \rangle^R(\mathbf{x}), \qquad (3.13)$$

where $\tilde{\theta}_1$ and $\tilde{\gamma}$ are given by (3.10) and (3.11). Because the updated functions are given by averages of bounded functions it is easily seen that they satisfy (2.3) for $\alpha = 1$ and for some non-negative constant K independent of $\mathbf{x}$.

The algorithm is guaranteed to converge due to the monotonic change of the objective under our choice of perturbation. The use of local averaging in the update scheme is similar to the use of filters in topology optimization; see (**34, 18**).

For points near the boundary a difficulty arises when defining the averages. This is dealt with by extending θ_1 and γ to the slightly larger domain $\Omega_R = \{\mathbf{x} \in \mathbb{R}^2; \text{dist}(\mathbf{x}, \Omega) \leqslant R\}$. The particular form of extension is up to the designer. Possibilities include setting $\theta_1 = 1$ and $\gamma = 0$ in $\Omega_R \backslash \Omega$ or reflection of θ_1, γ across the boundary of Ω into Ω_R. In the discretized problem used for the simulations we allow θ_1 and γ to take constant values inside each element and define $\langle \theta_1 \rangle^R$ and $\langle \gamma \rangle^R$ to be the averages of θ_1 and γ over neighbouring elements.

4. Numerical implementation for the X-shaped and L-shaped cross-sections

The first set of computational examples are carried out for an X-shaped domain. All interior angles for the reentrant corners are fixed at $3\pi/2$ radians. The shear stiffness of material one is assigned the value $G_1 = 1\,GPa$ and the shear stiffness of material two is assigned the value $G_2 = 2\,GPa$. For these choices $S_1 = 1/(2G_1) = 0.5$ and $S_2 = 1/(2G_2) = 0.25$. All of the design optimizations presented here are carried out with the area fraction of the compliant material held near 30 per cent of the total area of the shaft cross-section.

In Fig. 2(a), a grey scale plot of the local density $\hat{\theta}_1(\mathbf{x})$ of material one is given for an optimal design minimizing (3.1) subject to the penalization on $\int(f_1)$, so that $i = 1$ and $p = 1$ in (3.1). The darkest regions correspond to zones of composite containing the highest density of the compliant material, $\hat{\theta}_1 = 0.99$. The lightest zones correspond to regions where $\hat{\theta}_1 = 0.01$. In this design the most compliant material is placed next to the reentrant corners. In Fig. 2(b), the arrows representing the local layer normals $(\cos \hat{\gamma}(\mathbf{x}), \sin \hat{\gamma}(\mathbf{x}))$ are plotted for the optimal homogenized design.

In the next example we optimize for torsional rigidity only. The resulting design is referred to as design 1. The grey scale plot of $\hat{\theta}_1$ for this design is given in Fig. 3(a). Here the lightest region corresponds to the stiffest possible effective material with density $\hat{\theta}_1 = 0.01$. The darkest corresponds to the most compliant material with $\hat{\theta}_1 = 0.99$. As expected this design ignores the stress concentration at the reentrant corners and the stiffest material surrounds the compliant material in order to impart the greatest torsional rigidity to the structure. In the next example the torsional rigidity is optimized in the presence of an integral penalization $\int(f_1)^2$, so that $i = 1$ and $p = 2$ in (3.1). The plot of $\hat{\theta}_1$ for this design (design 2) is given in Fig. 4(a). For this case the more compliant material surrounds the stress concentration at the reentrant corners. In the final example the torsional rigidity is optimized in the presence of an integral penalization $\int(f_2)^2$, so that $i = 2$ and $p = 2$ in (3.1). The plot of $\hat{\theta}_1$ for this design (design 3) is given in Fig. 5(a). It is seen that the more compliant material surrounds the stress concentration at the reentrant corners. The associated torsional rigidities for all of these cases are listed in Table 1. It is seen from the table that the torsional rigidity drops for the penalized designs.

The contour plot of the macrostress modulation function f_1 for design 1 is given in Fig. 3(b). Figure 4(b) gives the contour plot for f_1 in design 2. When comparing designs 1 and 2 it is clear from Figs 3(b) and 4(b) that design 2 provides a significant reduction in the size of the overstressed zone $f_1 \geqslant 0.3$.

Note that Theorem 2.2 provides the method for constructing a locally layered material from the data given in design 2. The choice of partition $\mathcal{P}_{\tau^{N_0}}$ used in the construction can be obtained from any initially chosen partition after sufficient refinement of the initial partition; this is discussed in
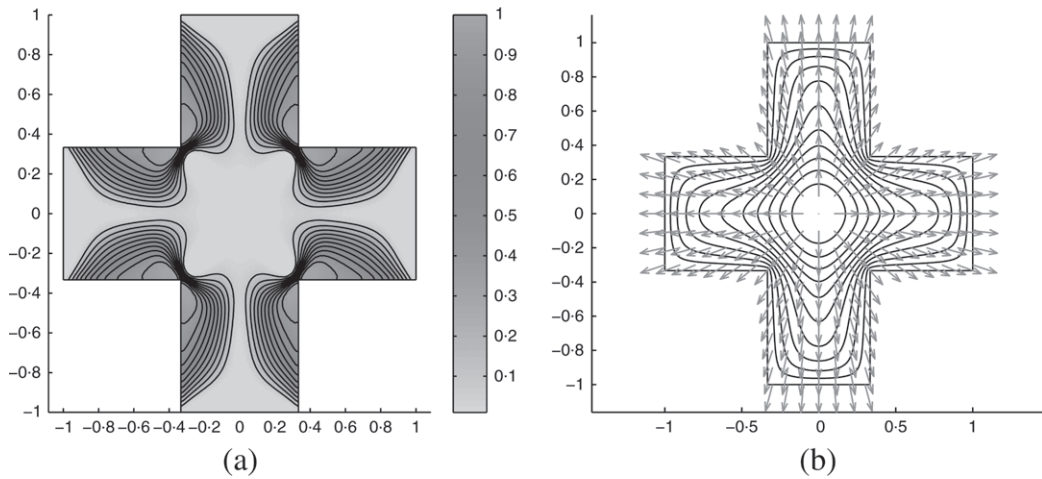
Fig. 2 (a) Density distribution of compliant material in X-shaped cross-section optimized for torsional rigidity with a $p = 1$ integral penalization on f_1. The darkest regions correspond to the most compliant material the lightest region corresponds to the location of the stiffest material. (b) Local layer directions and level lines of stress potential inside the X-shaped cross-section optimized for torsional rigidity with a $p = 1$ integral penalization on f_1
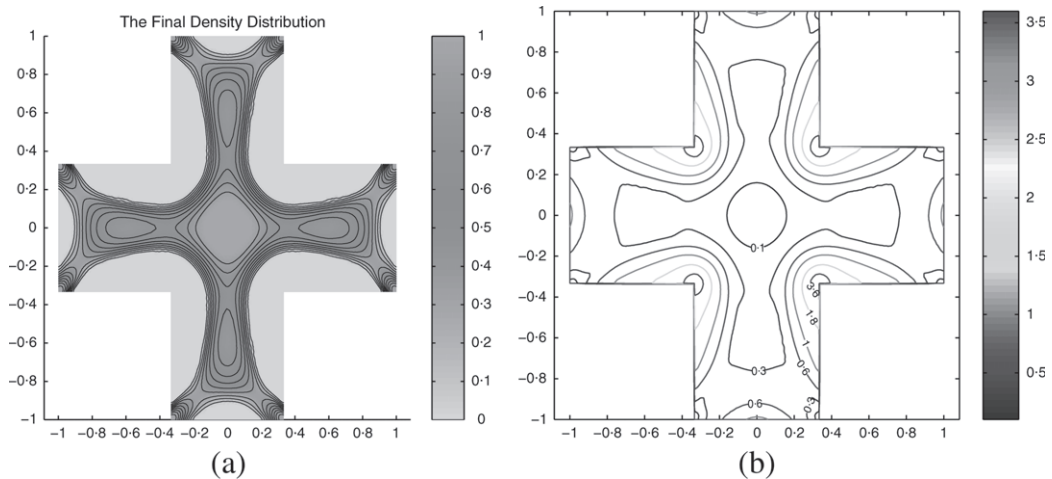

Fig. 3 Design 1. (a) Grey level plot of the density distribution of compliant material in X-shaped shaft cross-section optimized for torsional rigidity only. (b) Contour plot of f_1
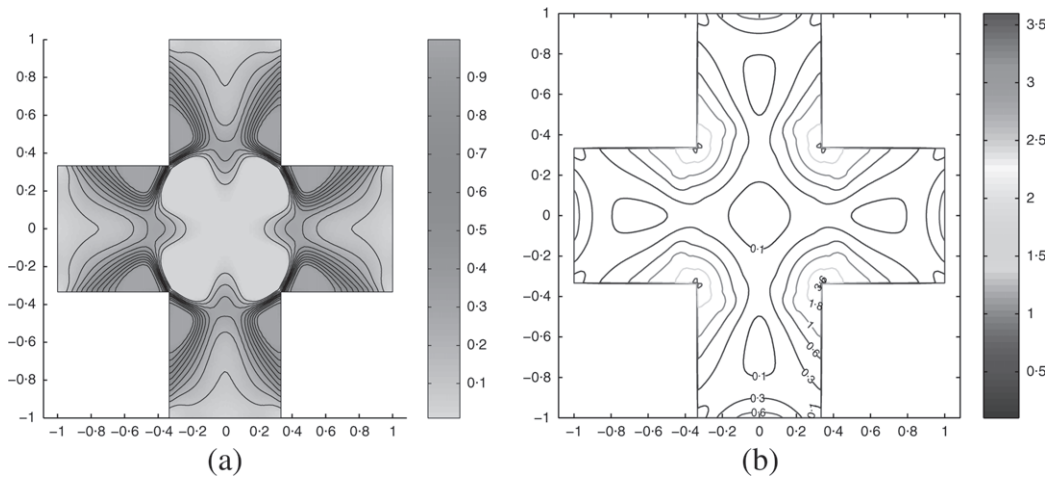
Fig. 4 Design 2. (a) Density distribution of compliant material in X-shaped cross-section optimized for torsional rigidity with $p = 2$ integral penalty on f_1. (b) Contour plot of f_1
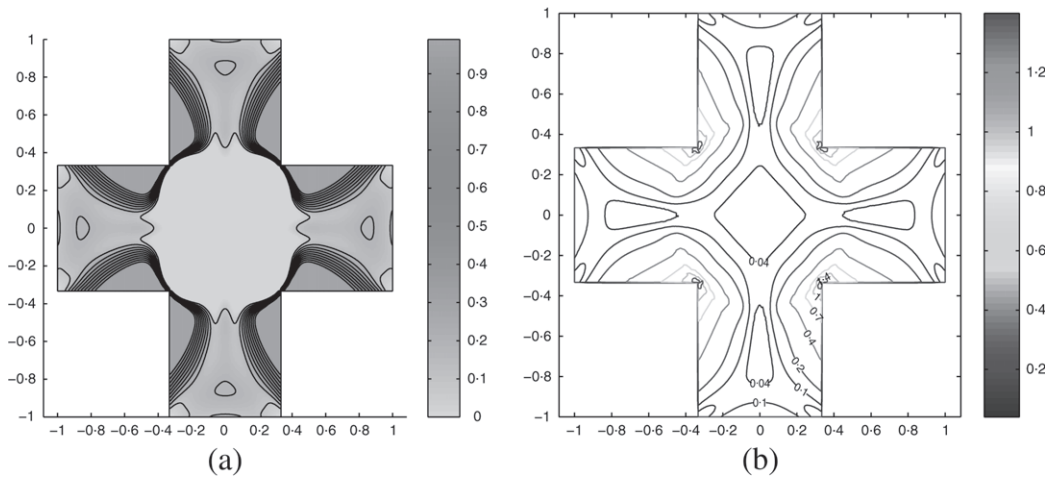

Fig. 5 Design 3. (a) Density distribution of compliant material in X-shaped cross-section optimized for torsional rigidity with $p = 2$ integral penalty on f_2. (b) Contour plot of f_2

Table 1   Results for X-shaped domains

Design number	Stress constraint	S_1-volume fraction	Torsional rigidity
1	None	30·8%	0·82
2	$\int (f_1)^2$	32·1%	0·61
3	$\int (f_2)^2$	30·1%	0·62

section 6. To fix ideas we choose a tolerance $\delta = 1/1000$ and $t = 0{\cdot}301$. Then Theorem 2.2 together with Remark 6.3 show how to construct a locally layered composite with layer thicknesses on a length scale $\varepsilon_0 > 0$ and torsional rigidity $\mathcal{R}^{\varepsilon_0, N_0}$ for which

$$|\mathcal{R}^{\varepsilon_0, N_0} - 0{\cdot}61| < 1/1000 \tag{4.1}$$

and for which the magnitude of the in-plane stress in material one lies below $0{\cdot}301$ for all points in the region $f_1 < 0{\cdot}3$ of Fig. 4(b), with the possible exception of a subset of points of area less than $1/1000$.

The contour plot of the macrostress modulation function f_2 is plotted in Fig. 6 for design 1. Figure 5(b) gives the contour plot of f_2 for design 3. An inspection of these figures shows that design 3 provides a significant reduction in the size of the overstressed zone $f_2 \geqslant 0{\cdot}1$ when compared to design 1.

Lastly we consider the L-shaped domain. In the first example for this domain we optimize for torsional rigidity only. The resulting design is referred to as design 4. The grey scale plot of $\hat{\theta}_1$ for this design is given in Fig. 7(a). Here the lightest region corresponds to the stiffest possible effective material with density $\hat{\theta}_1 = 0{\cdot}01$. The darkest corresponds to the most compliant material with $\hat{\theta}_1 = 0{\cdot}99$. As before this design ignores the stress concentration at the reentrant corners and the stiffest material surrounds the compliant material in order to impart the greatest torsional rigidity to the structure. In the next example the torsional rigidity is optimized in the presence of the integral penalization $\int (f_2)^2$. The plot of $\hat{\theta}_1$ for this design (design 5) is given in Fig. 8(a). It is seen that the more compliant material surrounds the stress concentration at the reentrant corners. The contour plot of the macrostress modulation function f_2 is plotted in Fig. 7(b) for design 4 and in Fig. 8(b) for design 5. Inspection of these figures shows that design 5 provides a significant reduction in the size of the overstressed zone $f_2 \geqslant 5{\cdot}0$ when compared to design 4. We point out that the torsional rigidity for design 4 is $3{\cdot}9$ while for design 5 it drops by almost half to $2{\cdot}0$. The examples show that the optimized designs for the L-shaped domain exhibit the same trends as the those for the X-shaped domain.

5. The optimal design for the homogenized design problem

We proceed using the direct method of the calculus of variations to show that there is an optimal design for the homogenized design problem presented in section 2. One starts by considering a minimizing sequence $\{\mathcal{B}_n\}_{n=1}^{\infty}$ for the homogenized design problem. The associated sequence of compliance tensors is denoted by $\{S^E(\mathcal{B}_n(\mathbf{x}))\}_{n=1}^{\infty}$ and the stress potentials $\{\phi_n^H\}_{n=1}^{\infty}$ vanish on the boundary of the cross-section and are solutions of

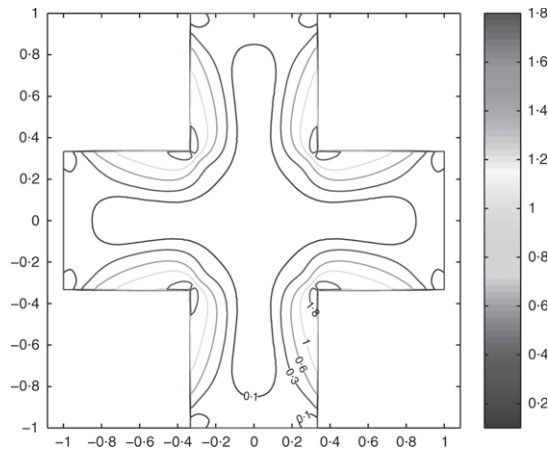$$-\operatorname{div}\left(S^E(\mathcal{B}_n)\nabla \phi_n^H\right) = 1 \tag{5.1}$$

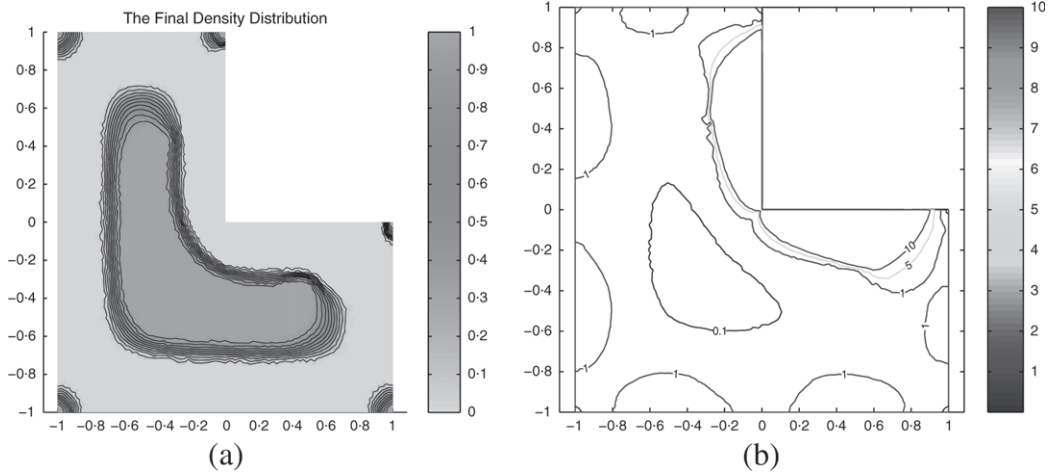**Fig. 6** Contour plot of f_2 for design 1

Fig. 7 Design 4. (a) Density distribution of compliant material in L-shaped cross-section optimized for torsional rigidity only. (b) Contour plot of f_2

satisfying the stress constraints

$$f_i(\mathcal{B}_n, \nabla\phi_n^H) \leqslant T^2 \quad \text{for } i = 1, 2 \tag{5.2}$$

over the set $\mathcal{S}$ and

$$HP = \lim_{n\to\infty} 2 \int_\Omega \phi_n^H \, dx_1 \, dx_2. \tag{5.3}$$
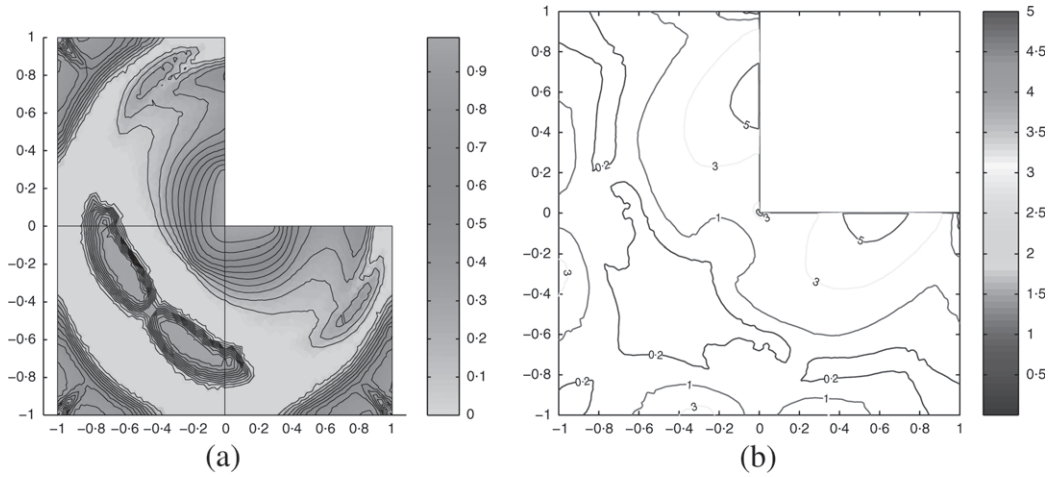
Fig. 8 Design 5. (a) Density distribution of compliant material in L-shaped cross-section optimized for torsional rigidity subject to rigidity with $p = 2$ integral penalty on f_2. (b) Contour plot of f_2

Since $\{\mathcal{B}_n(\mathbf{x})\}_{n=1}^{\infty}$ is an equicontinuous family of functions over the closure of Ω one readily deduces that there is a subsequence, also denoted by $\{\mathcal{B}_n(\mathbf{x})\}_{n=1}^{\infty}$, converging uniformly in Ω to a design $\hat{\mathcal{B}}$ in $\mathcal{D}_\Theta$. This delivers the convergence

$$\lim_{n\to\infty} S^E(\mathcal{B}_n(\mathbf{x})) = S^E(\hat{\mathcal{B}}(\mathbf{x})) \quad \text{and} \quad \lim_{n\to\infty} f_i(\mathcal{B}_n(\mathbf{x}), \mathbf{v}) \geqslant f_i(\hat{\mathcal{B}}(\mathbf{x}), \mathbf{v}), \quad i = 1, 2, \qquad (5.4)$$

for every point $\mathbf{x}$ in the domain. From the theory of G-convergence (**35**) and H-convergence (**36**) one has that the sequence $\{\phi_n^H\}_{n=1}^{\infty}$ converges weakly in the Sobolev space $W_0^{1,2}(\Omega)$ to the stress potential $\hat{\phi}^H$ associated with $S^E(\hat{\mathcal{B}})$, where

$$-\operatorname{div}\left(S^E(\hat{\mathcal{B}})\nabla\hat{\phi}^H\right) = 1 \qquad (5.5)$$

and

$$\lim_{n\to\infty} 2\int_\Omega \phi_n^H \, dx_1 \, dx_2 = 2\int_\Omega \hat{\phi}^H \, dx_1 \, dx_2. \qquad (5.6)$$

To conclude the proof one checks to see if the homogenized stress constraints (2.12) are satisfied by the stress associated with $\hat{\mathcal{B}}$. Since the sequence $\{S^E(\mathcal{B}_n(\mathbf{x}))\}_{n=1}^{\infty}$ converges pointwise to $S^E(\hat{\mathcal{B}}(\mathbf{x}))$ the sequence of gradients $\{\nabla\phi_n^H\}_{n=1}^{\infty}$ converge strongly in $L^2(\Omega)^2$ to $\nabla\hat{\phi}^H$; see (**35**). Passing to a subsequence if necessary, also denoted by $\{\nabla\phi_n^H\}_{n=1}^{\infty}$, it follows that this subsequence converges pointwise to $\nabla\hat{\phi}^H$. From this one deduces that

$$T^2 \geqslant \lim_{n\to\infty} f_i(\mathcal{B}_n, \nabla\phi_n^H) \geqslant f_i(\hat{\mathcal{B}}, \nabla\hat{\phi}^H) \quad \text{for } i = 1, 2 \qquad (5.7)$$

for almost every point and Theorem 2.1 is established.

The proof of Theorem 3.1 follows the same steps. As before one concludes that the minimizing sequence $\{\mathcal{B}_n(\mathbf{x})\}_{n=1}^{\infty}$ of designs for (3.1) converge uniformly to the limit $\hat{\mathcal{B}}$ where $\hat{\mathcal{B}}$ is in D_θ. Here the associated stress potentials $\{\phi_n^H\}_{n=1}^{\infty}$ satisfy

$$\lim_{n\to\infty} 2\int_\Omega \phi_n^H \, dx_1 \, dx_2 = 2\int_\Omega \hat{\phi}^H \, dx_1 \, dx_2 = R(\hat{\mathcal{B}}) \qquad (5.8)$$

and the pointwise convergence

$$\lim_{n\to\infty} \nabla\phi_n^H(\mathbf{x}) = \nabla\hat{\phi}^H(\mathbf{x}) \text{ a.e.,} \tag{5.9}$$

where

$$-\operatorname{div}\left(S^E(\hat{\mathcal{B}})\nabla\hat{\phi}^H\right) = 1. \tag{5.10}$$

Last, Fatou's lemma gives

$$\int_\Omega f_i(\hat{\mathcal{B}}(x), \nabla\hat{\phi}^H))^p \, dx \leqslant \liminf_{n\to\infty} \int_\Omega (f_i(\mathcal{B}_n(x), \nabla\phi_n^H))^p \, dx, \ i = 1, 2, \tag{5.11}$$

and Theorem 3.1 follows.

6. Identifying locally layered microgeometry with desirable strength and stiffness properties

In this section, Theorem 2.2 is established. The proof is based on two steps. First, a version of the identification theorem is established (Theorem 6.2) for the case when the design vector $\mathcal{B}(\mathbf{x})$ takes piecewise constant values. Secondly, Theorem 2.2 is established by using a sequence of piecewise constant approximations to the optimal design vector $\hat{\mathcal{B}}$.

Consider a partition of the shaft cross-section $\mathcal{P}_{\tau^N}$ with the subsets in the partition denoted by ω_N^k, $k = 1, \ldots, N$. We follow the standard convention in the theory of finite elements and take the subsets in the partition to be open such that the union of their closures is equal to the closure of the set Ω describing the cross-section. Denoting the piecewise constant design vector by $\mathcal{B}_N(\mathbf{x})$ we suppose that it takes the constant values $(\theta_{1N}^k, \gamma_N^k)$ for $\mathbf{x}$ inside each subdomain ω_N^k. Here θ_{1N}^k and γ_N^k satisfy the box constraints given by (2.13). The associated compliance tensor $S^E(\mathcal{B}_N)$ is piecewise constant and the stress potential ϕ^N vanishes on the boundary and is the solution of

$$-\operatorname{div}\left(S^E(\mathcal{B}_N)\nabla\phi^N\right) = 1.$$

Suppose we are given that $\nabla\phi^N$ satisfies the stress constraints given by

$$f_i(\mathcal{B}_N, \nabla\phi^N) \leqslant \tau^2 \quad \text{for } i = 1, 2 \quad \text{and} \quad \mathbf{x} \text{ in } \omega, \tag{6.1}$$

where ω is a subset of the cross-section. Here the distance between any point inside ω and the boundary of the cross-section is greater than some fixed positive number. Next consider the locally layered microstructure with the thickness of the stiff layers and compliant layers given by $\varepsilon\theta_{1N}^k$ and $\varepsilon\theta_{2N}^k$ respectively in ω_N^k. The layer normals are specified by γ_N^k in ω_N^k. The associated piecewise constant compliance is given by $S^{\varepsilon,N} = S_1\chi_1^{\varepsilon,N} + S_2\chi_2^{\varepsilon,N}$. The stress potential in the shaft cross-section filled with locally layered material is denoted by $\phi^{\varepsilon,N}$. The stress potential vanishes on the boundary and is a solution of

$$-\operatorname{div}\left(S^{\varepsilon,N}\nabla\phi^{\varepsilon,N}\right) = 1.$$

DEFINITION 6.1. For $t \geqslant 0$ we introduce the distribution function $\lambda_i^{\varepsilon,N}(t, \omega)$ which gives the Lebesgue measure (area) of the set of points in ω where $\chi_i^{\varepsilon,N}|\nabla\phi^{\varepsilon,N}| > t$, $i = 1, 2$.

THEOREM 6.2. *Suppose that the homogenized stress constraint (6.1) holds. Then, on passage to a subsequence if necessary, the sequence of stress potentials* $\{\phi^{\varepsilon,N}\}_{\varepsilon>0}$ *has the following two*

properties:

$$\lim_{\varepsilon \to 0} 2 \int_{\Omega} \phi^{\varepsilon,N} \, dx_1 \, dx_2 = 2 \int_{\Omega} \phi^N \, dx_1 \, dx_2 \tag{6.2}$$

and

$$\lim_{\varepsilon \to 0} \lambda_i^{\varepsilon,N}(t, \omega) = 0 \quad \text{for } t > \tau. \tag{6.3}$$

Note here that (6.3) states that for any $t > \tau > 0$, the area of the part of ω over which $\chi_1^{\varepsilon,N} |\nabla \phi^{\varepsilon,N}| > t$ and $\chi_2^{\varepsilon,N} |\nabla \phi^{\varepsilon,N}| > t$ vanishes as $\varepsilon \to 0$.

Proof. The sequence $\{S^{\varepsilon,N}\}_{\varepsilon > 0}$ associated with locally layered geometries converges in homogenization to $S^E(\mathcal{B}_N)$; see (**3**). Consequently the sequence of potentials $\{\phi^{\varepsilon,N}\}_{\varepsilon > 0}$ converges weakly in $W_0^{1,2}(\Omega)$ to ϕ^N and (6.2) follows. To establish (6.3), we introduce the characteristic function $\chi_{i,t}^{\varepsilon,N}$ of the set of points in Ω where $\chi_i^{\varepsilon,N} |\nabla \phi^{\varepsilon,N}| > t$, $i = 1, 2$. Here

$$\lambda_i^{\varepsilon,N}(t, \omega) = \int_{\omega} \chi_{i,t}^{\varepsilon,N} \, dx_1 \, dx_2. \tag{6.4}$$

From the theory of weak convergence (**37**) one passes to a subsequence if necessary to assert the existence of a density $\theta_{i,t}^N$ for which

$$\lim_{\varepsilon \to 0} \lambda_i^{\varepsilon,N}(t, \omega) = \int_{\omega} \theta_{i,t}^N \, dx_1 \, dx_2. \tag{6.5}$$

Here, $0 \leqslant \theta_{i,t}^N \leqslant 1$. In physical terms $\theta_{i,t}^N$ can be thought of as giving the distribution of states for the stress in the homogenized composite. The derivative of $\theta_{i,t}^N$ with respect to t gives the density of states. For any point $\mathbf{x}$ inside the cross-section we introduce the sequence of squares centred at $\mathbf{x}$ with side length $\ell_j = 1/j$, $j = 1, 2, \ldots$ denoted by $Q(\mathbf{x}, j)$. For j large enough the squares are contained inside ω. We test the microstructure inside the squares by imposing two linearly independent unit loads given by $\mathbf{e}^1 = (1, 0)$ and $\mathbf{e}^2 = (0, 1)$ and track the stress fluctuations inside the square as ε tends to zero. Mathematically this is done by keeping track of the $Q(\mathbf{x}, j)$ periodic stress potentials $w_m^{\varepsilon,j,N}$ that solve

$$\operatorname{div}\left(S^{\varepsilon,N}(\nabla w_m^{\varepsilon,j,N} + \mathbf{e}^m)\right) = 0 \quad \text{for } m = 1, 2. \tag{6.6}$$

For $\mathbf{y}$ in $Q(\mathbf{x}, j)$ we introduce the fluctuation matrix $Q_{mn}^{i,\varepsilon,j,N}(\mathbf{y})$ defined by

$$Q_{mn}^{i,\varepsilon,j,N}(\mathbf{y}) = \chi_i^{\varepsilon,N}(\mathbf{y})(\nabla w_m^{\varepsilon,j,N}(\mathbf{y}) + \mathbf{e}^m) \cdot (\nabla w_n^{\varepsilon,j,N}(\mathbf{y}) + \mathbf{e}^n). \tag{6.7}$$

From (**31**, Lemma 3.7) one has

$$t^2 \theta_{i,t}^N(\mathbf{x}) \leqslant M^{i,N}(\mathbf{x}) \nabla \phi^N(\mathbf{x}) \cdot \nabla \phi^N(\mathbf{x}) \quad \text{a.e.,} \tag{6.8}$$

where the tensor $M^{i,N}(\mathbf{x})$ is defined by

$$M^{i,N}(\mathbf{x}) = \lim_{j \to \infty} \lim_{\varepsilon \to 0} \frac{1}{|Q(\mathbf{x}, j)|} \int_{Q(\mathbf{x},j)} \chi_{i,t}^{\varepsilon,N}(\mathbf{y}) Q^{i,\varepsilon,j,N}(\mathbf{y}) \, dy_1 \, dy_2. \tag{6.9}$$

We now develop an upper bound on $M^{i,N}(\mathbf{x})$ that is given in terms of $\theta_{i,t}^N(\mathbf{x})$ and $f_i(\mathcal{B}_N, \nabla \phi^N(\mathbf{x}))$. It is supposed that $\mathbf{x}$ lies in one of the subsets of the partition. This is true for almost every point in the cross-section. Without loss of generality suppose this subset is ω_N^k. For ℓ_j sufficiently small

$Q(\mathbf{x}, j)$ is compactly contained inside ω_N^k and we apply the corrector theory given in (**36**) to easily deduce that

$$\nabla w_m^{\varepsilon, j, N}(\mathbf{y}) + \mathbf{e}^m = P^{\varepsilon, k, N}(\mathbf{y})\mathbf{e}^m + r^{\varepsilon, j, k, N}, \tag{6.10}$$

where

$$r^{\varepsilon, j, k, N} \to 0 \tag{6.11}$$

in mean square over $Q(\mathbf{x}, j)$. For $\mathbf{y}$ in $Q(\mathbf{x}, j)$, the corrector matrix is given by

$$P^{\varepsilon, k, N}(\mathbf{y}) = \chi_1^{\varepsilon, N}(\mathbf{y})R(\gamma_N^k)\Lambda^1(\theta_{1N}^k)R^T(\gamma_N^k) + \chi_2^{\varepsilon, N}(\mathbf{y})R(\gamma_N^k)\Lambda^2(\theta_{1N}^k)R^T(\gamma_N^k). \tag{6.12}$$

From (6.9) to (6.12) one sees that

$$M^{i, N}(\mathbf{x}) = \lim_{j \to \infty} \lim_{\varepsilon \to 0} \frac{1}{|Q(\mathbf{x}, j)|} \int_{Q(\mathbf{x}, j)} \chi_{i, t}^{\varepsilon, N}(\mathbf{y})\chi_i^{\varepsilon, N}(\mathbf{y})Q_i(\mathcal{B}_N)\, dy_1\, dy_2, \quad i = 1, 2,$$

where $Q_i(\mathcal{B})$, $i = 1, 2$, are given by (2.8) and (2.9).

In order to facilitate the exposition we provide an explicit formula for the characteristic functions $\chi_i^{\varepsilon, N}$ in terms of the local layer normal and volume fraction. Let a be a number in $[0, 1]$ and define periodic functions on $[0, 1]$ denoted by $\chi_1(a, s)$ and $\chi_2(a, s)$ such that $\chi_1(a, s) = 1$ for $0 \leqslant s < a$, $\chi_1(a, s) = 0$ for $a \leqslant s \leqslant 1$ and $\chi_2(a, s) = 1 - \chi_1(a, s)$. Then for $\mathbf{x}$ in ω_N^k one writes $\chi_i^{\varepsilon, N} = \chi_i(\theta_1^k, \mathbf{n}^k \cdot \mathbf{x}/\varepsilon)$. We apply Hölder's inequality to deduce that

$$M^{i, N}(\mathbf{x})\nabla\phi^N(\mathbf{x}) \cdot \nabla\phi^N(\mathbf{x}) \leqslant \lim_{j \to \infty} \lim_{\varepsilon \to 0} \frac{1}{|Q(\mathbf{x}, j)|} \int_{Q(\mathbf{x}, j)} \chi_{i, t}^{\varepsilon, N}(\mathbf{y})\, dy_1\, dy_2$$

$$\times \operatorname*{esssup}_{0 \leqslant s \leqslant 1}\left\{\chi_i(\theta_1^k, s)Q_i(\mathcal{B}_N)\nabla\phi^N(\mathbf{x}) \cdot \nabla\phi^N(\mathbf{x})\right\}$$

$$= \theta_{i, t}^N(\mathbf{x})f_i(\mathcal{B}_N, \nabla\phi^N(\mathbf{x})), \tag{6.13}$$

where

$$\theta_{i, t}^N(\mathbf{x}) = \lim_{j \to \infty} \lim_{\varepsilon \to 0} \frac{1}{|Q(\mathbf{x}, j)|} \int_{Q(\mathbf{x}, j)} \chi_{i, t}^{\varepsilon, N}(\mathbf{y})\, dy_1\, dy_2 \tag{6.14}$$

holds for almost every point in ω and $f_i(\mathcal{B}_N, \mathbf{v})$ are the macrostress modulations defined by (2.10) and (2.11).

The inequality (6.8) together with (6.13) delivers the homogenization constraint

$$\theta_{i, t}^N(\mathbf{x})\left(f_i(\mathcal{B}_N, \nabla\phi^N) - t^2\right) \geqslant 0, \quad i = 1, 2, \tag{6.15}$$

for $t > 0$ and almost every $\mathbf{x}$ in ω.

In what follows we will denote the measure (area) of a set G by $|G|$. The set of points in ω for which $\theta_{i, t}^N(\mathbf{x}) > 0$ is denoted by $\{\theta_{i, t}^N > 0\}$ and the set of points in ω for which $f_i(\mathcal{B}_N, \nabla\phi^N) \geqslant t^2$ is denoted by $\{f_i \geqslant t^2\}$. From (6.15) it is evident that almost every point in $\{\theta_{i, t}^N > 0\}$ also belongs to $\{f_i \geqslant t^2\}$ so

$$|\{\theta_{i, t}^N > 0\}| \leqslant |\{f_i \geqslant t^2\}|. \tag{6.16}$$

It follows that

$$\lim_{\varepsilon \to 0} \lambda_i^{\varepsilon, N}(t, \omega) = \int_\omega \theta_{i, t}^N\, dx_1\, dx_2 \leqslant |\{\theta_{i, t}^N > 0\}| \tag{6.17}$$

and from (6.16) we deduce that

$$\lim_{\varepsilon \to 0} \lambda_i^{\varepsilon, N}(t, \omega) \leqslant |\{f_i \geqslant t^2\}| \tag{6.18}$$

and it is clear that

$$\lim_{\varepsilon \to 0} \lambda_i^{\varepsilon, N}(t, \omega) = 0 \tag{6.19}$$

if

$$f_i(\mathcal{B}_N, \nabla \phi^N) < t^2 \quad \text{for all points } \mathbf{x} \text{ in } \omega; \tag{6.20}$$

Theorem 6.2 is proved.

In order to expedite the presentation we call any partition $\mathcal{P}_{\tau^M}$ of the shaft into M subdomains with $M > N$ a refinement of $\mathcal{P}_{\tau^N}$ if $\tau_N \geqslant \tau_M$, and if every set in the partition $\mathcal{P}_{\tau^M}$ is a subset of a set belonging to $\mathcal{P}_{\tau^N}$. Now for a given partition $\mathcal{P}_{\tau^N}$ consider a sequence of refinements $\{\mathcal{P}_{\tau^{N_j}}\}_{j=1}^{\infty}$ such that $\mathcal{P}_{\tau^{N_{j+1}}}$ is a refinement of $\mathcal{P}_{\tau^{N_j}}$ with $\mathcal{P}_{\tau^{N_1}} = \mathcal{P}_{\tau^N}$. Here $\tau^{N_j} \to 0$ as $j \to \infty$. The sets belonging to $\mathcal{P}_{\tau^{N_j}}$ are denoted by $\omega_{N_j}^k$, $k = 1 \ldots, N_j$.

Recall the optimal design $\hat{\mathcal{B}}$ and let $\mathcal{B}_{N_j}$ denote the piecewise constant design vector taking values $(\theta_{N_j}^k, \gamma_{N_j}^k)$ determined by the averages

$$\hat{\theta}_{1\,N_j}^k = \frac{1}{\text{Area of } \omega_{N_j}^k} \int_{\omega_{N_j}^k} \hat{\theta}_1(\mathbf{x}) \, dx_1 \, dx_2, \quad \hat{\gamma}_{N_j}^k = \frac{1}{\text{Area of } \omega_{N_j}^k} \int_{\omega_{N_j}^k} \hat{\gamma}(\mathbf{x}) \, dx_1 \, dx_2.$$

Associated with $\mathcal{B}_{N_j}$ is the piecewise constant compliance tensor $S^E(\mathcal{B}_{N_j})$ and stress potential ϕ^{N_j} that vanishes on the boundary of the cross-section and satisfies

$$- \text{div}\big(S^E(\mathcal{B}_{N_j}) \nabla \phi^{N_j}\big) = 1. \tag{6.21}$$

We consider the intersection of the set of Lebesgue points for each of the functions $\hat{\theta}_1$ and $\hat{\gamma}$. On this set $\mathcal{B}_{N_j} \to \hat{\mathcal{B}}$ as $j \to \infty$. This delivers the convergence

$$\lim_{j \to \infty} S^E(\mathcal{B}_{N_j}) = S^E(\hat{\mathcal{B}}) \quad \text{for almost every } \mathbf{x} \text{ in } \Omega. \tag{6.22}$$

Define $\hat{\theta}_2 = 1 - \hat{\theta}_1$ and for almost every point for which $\hat{\theta}_i(\mathbf{x}) > 0$ one has that

$$\lim_{j \to \infty} f_i(\mathcal{B}_{N_j}(\mathbf{x}), \mathbf{v}) = f_i(\hat{\mathcal{B}}(\mathbf{x}), \mathbf{v}), \tag{6.23}$$

otherwise over almost every point for which $\hat{\theta}_i(\mathbf{x}) = 0$ one has

$$\lim_{j \to \infty} f_i(\mathcal{B}_{N_j}(\mathbf{x}), \mathbf{v}) \geqslant f_i(\hat{\mathcal{B}}(\mathbf{x}), \mathbf{v}) = 0. \tag{6.24}$$

It follows immediately from the theory of homogenization (**35**, **36**) that $\{\phi^{N_j}\}_{j=1}^{\infty}$ converges weakly in $W_0^{1,2}$ to $\hat{\phi}^H$ and

$$\lim_{j \to \infty} \int_{\Omega} \phi^{N_j} \, dx_1 \, dx_2 = \int_{\Omega} \hat{\phi}^H \, dx_1 \, dx_2. \tag{6.25}$$

Moreover since the sequence of tensors $\{S^E(\mathcal{B}_{N_j})\}_{j=1}^{\infty}$ converge pointwise to $S^E(\hat{\mathcal{B}})$, standard arguments show that the sequence $\{\nabla \phi^{N_j}\}_{j=1}^{\infty}$ converges in mean square to $\nabla \hat{\phi}^H$. On passing

to a subsequence if necessary one may assume that the sequence $\{\nabla\phi^{N_j}\}_{j=1}^{\infty}$ converges almost everywhere to $\nabla\hat{\phi}^H$.

We partition the set $\mathcal{S}$ into two subsets $\mathcal{S}_i^0$ and $\mathcal{S}_i^+$ where $\hat{\theta}_i = 0$ on $\mathcal{S}_i^0$ and $\hat{\theta}_i > 0$ on $\mathcal{S}_i^+$. Collecting observations one readily sees that

$$\lim_{j\to\infty} f_i(\mathcal{B}_{N_j}(\mathbf{x}), \nabla\phi^{N_j}(\mathbf{x})) = f_i(\hat{\mathcal{B}}(\mathbf{x}), \nabla\hat{\phi}^H(\mathbf{x})) \tag{6.26}$$

for almost every $\mathbf{x}$ in $\mathcal{S}_i^+$ and

$$\lim_{j\to\infty} f_i(\mathcal{B}_{N_j}(\mathbf{x}), \nabla\phi^{N_j}(\mathbf{x})) \geqslant f_i(\hat{\mathcal{B}}(\mathbf{x}), \nabla\hat{\phi}^H(\mathbf{x})) = 0 \tag{6.27}$$

for almost every $\mathbf{x}$ in $\mathcal{S}_i^0$.

Next consider the sequence of piecewise locally layered microstructures associated with $S^E(\mathcal{B}_{N_j})$ constructed according to the hypotheses of Theorem 6.2. The sequence of stress potentials for these microstructures is denoted by $\{\phi^{\varepsilon,N_j}\}_{j=1}^{\infty}$. From Theorem 6.2 and (6.25) it follows immediately that

$$\lim_{j\to\infty}\lim_{\varepsilon\to 0}\int_{\Omega}\phi^{\varepsilon,N_j}\,dx_1\,dx_2 = \int_{\Omega}\hat{\phi}^H\,dx_1\,dx_2 = \mathcal{R}(\hat{\mathcal{B}}). \tag{6.28}$$

Standard arguments show that for any subset C of Ω

$$\lim_{j\to\infty}\lim_{\varepsilon\to 0}\int_{C}\chi_i^{\varepsilon,N_j}\,dx_1\,dx_2 = \lim_{j\to\infty}\int_{C}\theta_i^{N_j}\,dx_1\,dx_2 = \int_{C}\hat{\theta}_i\,dx_1\,dx_2. \tag{6.29}$$

In order to finish the proof of Theorem 2.2, it remains to show that for $t > T$ the associated sequence of distribution functions $\lambda_i^{\varepsilon,N_j}(t,\mathcal{S})$ satisfies

$$\lim_{j\to\infty}\lim_{\varepsilon\to 0}\lambda_i^{\varepsilon,N_j}(t,\mathcal{S}) = 0, \quad i = 1, 2. \tag{6.30}$$

We write $\mathcal{S} = \mathcal{S}_i^0 \cup \mathcal{S}_i^+$ and note that

$$\lim_{j\to\infty}\lim_{\varepsilon\to 0}\lambda_i^{\varepsilon,N_j}(t,\mathcal{S}) = \lim_{j\to\infty}\lim_{\varepsilon\to 0}\lambda_i^{\varepsilon,N_j}(t,\mathcal{S}_i^0) + \lim_{j\to\infty}\lim_{\varepsilon\to 0}\lambda_i^{\varepsilon,N_j}(t,\mathcal{S}_i^+), \quad i = 1, 2.$$

We then observe that the inequality $\chi_{i,t}^{\varepsilon,N_j} \leqslant \chi_i^{\varepsilon,N_j}$ together with (6.29) gives

$$\lim_{j\to\infty}\lim_{\varepsilon\to 0}\lambda_i^{\varepsilon,N_j}(t,\mathcal{S}_i^0) = 0. \tag{6.31}$$

We choose τ so that $T < \tau < t$. Setting

$$A_{N_j}^{\tau} = \{\mathbf{x} \text{ in } \mathcal{S}_i^+ ; \; f_i(\mathcal{B}_{N_j}(\mathbf{x}), \nabla\phi^{N_j}(\mathbf{x})) > \tau^2\} \tag{6.32}$$

it is evident from (6.26) and

$$f_i(\hat{\mathcal{B}}(\mathbf{x}), \nabla\hat{\phi}^H(\mathbf{x})) \leqslant T^2 \quad \text{for } i = 1, 2 \tag{6.33}$$

that $\lim_{j\to\infty} |A_{N_j}^{\tau}| = 0$ for $\tau > T$. The points in $\mathcal{S}_i^+$ not in $A_{N_j}^{\tau}$ are denoted by $\mathcal{S}_i^+ \backslash A_{N_j}^{\tau}$. On this set $f_i(\mathcal{B}_{N_j}(\mathbf{x}), \nabla\phi^{N_j}(\mathbf{x})) \leqslant \tau^2$ and from Theorem 6.2 we deduce that

$$\lim_{\varepsilon\to 0} \lambda_i^{\varepsilon, N_j}(t, \mathcal{S}_i^+ \backslash A_{N_j}^{\tau}) = 0. \tag{6.34}$$

Lastly it is evident that $\lambda_i^{\varepsilon, N_j}(t, A_{N_j}^{\tau}) \leqslant |A_{N_j}^{\tau}|$ and (6.30) follows after taking limits, since

$$\lambda_i^{\varepsilon, N_j}(t, \mathcal{S}_i^+) = \lambda_i^{\varepsilon, N_j}(t, A_{N_j}^{\tau}) + \lambda_i^{\varepsilon, N_j}(t, \mathcal{S}_i^+ \backslash A_{N_j}^{\tau}) \tag{6.35}$$

and Theorem 2.2 is established.

REMARK 6.3 The proof of Theorem 2.2 contains the algorithm for selecting the partition used in the construction of a locally layered microstructure that satisfies the design requirements given by (2.18) to (2.20). Indeed one can choose any initial partition denoted by $\mathcal{P}_{\tau N}$ and consider the sequence of refinements $\{\mathcal{P}_{\tau^{N_j}}\}_{j=1}^{\infty}$, where $\mathcal{P}_{\tau^{N_1}} = \mathcal{P}_{\tau N}$ and $\lim_{j\to\infty} \tau^{N_j} = 0$. For given tolerances $t > T$ and $\delta > 0$ it follows from (6.28) to (6.30) that there exist a sufficiently refined partition $\mathcal{P}_{\tau^{N_{\hat{j}}}}$ for which one can choose a locally layered microstructure on a sufficiently fine length scale ε_0 that satisfies the design requirements (2.18) to (2.20).

7. Conclusion

The inverse homogenization design method provides a means to construct a locally layered material with desired strength and stiffness properties with layer thicknesses on a sufficiently small length scale $\varepsilon_0 > 0$. However this methodology does not give a priori information on what this length scale should be. To fix ideas we identify some of the relevant quantities influencing the length scale for the simple case of a smooth domain containing a uniform microgeometry. We consider a smooth domain Ω containing a layered material with the scale of the layers being ε. The associated stress potential is denoted by ϕ^{ε} and the homogenized stress potential is denoted by ϕ^H. The distribution function $\lambda_i^{\varepsilon}(t)$ gives the measure of the set inside the ith material, where $|\nabla\phi^{\varepsilon}| > t$. We suppose that it is known that $f_i(\mathcal{B}, \nabla\phi^H) \leqslant T^2$ in Ω. For this case one can apply well-known results in corrector theory (**38**) to deduce a bound on the distribution function given by

$$\lambda_i^{\varepsilon}(\tau + \varepsilon h) \leqslant \frac{\sqrt{\varepsilon} \left(C_1 \max_{\mathbf{x} \text{ in } \Omega} \{|\nabla\nabla\phi^H(\mathbf{x})|\} + B_1 \max_{\mathbf{x} \text{ in } \Omega} \{|\nabla\phi^H(\mathbf{x})|\} \right)}{\tau - T}$$

for $\tau > T$, where $h = C_2 \max_{\mathbf{x} \text{ in } \Omega} \{|\nabla\nabla\phi^H(\mathbf{x})|\} + B_2 \max_{\mathbf{x} \text{ in } \Omega} \{|\nabla\phi^H(\mathbf{x})|\}$ and where C_1, C_2, B_1 and B_2 depend on the area fraction and shear moduli of each of the materials and ε independent norms of boundary-layer functions. From this estimate it is clear that the homogenized stress and stress gradient $\nabla\nabla\phi^H$ together with boundary layers play a strong role in determining the length scale ε_0 of the microstructured material possessing the desired properties. Future work will focus on a priori estimates for this length scale for graded composite materials while keeping in mind the singularity strength associated with reentrant corners and the wavelength of the loading.

   The numerical method presented here can be applied to the design of locally layered microstructures for fully three-dimensional linear elastic problems. This can be justified following the methods developed in this paper. The only technical modification necessary to justify the method for the three-dimensional case is to replace the convergence result described by (6.10) and (6.11) with the analogous one suitable for the system of linear elasticity. Such a convergence result follows directly from the work of (**39**).

Acknowledgments

References

1. K. A. Lurie and A. V. Cherkaev, Non-homogeneous bar of extremal torsional rigidity, *Nonlinear Problems of Structural Mechanics, Structural Optimization* (Naukowa Dumka, Kiev 1978) 64–68.

2. K. T. Cheng and N. Olhoff, An investigation concerning optimal design of solid elastic plates, *Int. J. Sol. Str.* **17** (1981) 305–323.

3. F. Murat and L. Tartar, Calcul des variations et homogénéisation, *Les Méthodes de l'Homogénéisation: Théorie et Applications en Physique*. Ecole d'Eté d'Analyse Numérique C.E.A.-E.D.F.-INRIA (Bréau-sans-Nappe, 1983), Collection de la Direction des Études et Recherches d'Electricité de France 57 (Eyrolles, Paris 1985) 319–369.

4. K. A. Lurie and A. V. Cherkaev, Effective characteristics of composite materials and the optimal design of structural elements, *Uspekhi Mekhaniki* (*Advances in Mechanics*) **9**:2 (1986) 3–81.

5. M. P. Bendsøe and N. Kikuchi, Generating optimal topologies in structural design using a homogenization method, *Comput. Methods Appl. Mech. Engrg* **71** (1988) 197–224.

6. A. R. Diaz and N. Kikuchi, Solutions to shape and topology eigenvalue optimization problems using a homogenization method, *Int. J. Numer. Meth. Engng* **35** (1992) 1487–1502.

7. G. Allaire and R. V. Kohn, Optimal design for minimum weight and compliance in plane stress using extremal microstructure, *Euro. J. Mech.* **12** (1993) 839–878.

8. O. Sigmund and S. Torquato, Design of materials with extreme thermal expansion using a three-phase topology optimization method, *J. Mech. Phys. Solids* **45** (1997) 1037–1067.

9. A. R. Diaz and R. Lipton, Optimal material layout for three-dimensional elastic structures subject to multiple loads, *Mech. Struct. and Mach.* **28** (2000) 219–236.

10. D. Fujii, B. C. Chen and N. Kikuchi, Composite material design of two-dimensional structures using the homogenization design method, *Int. J. Numer. Meth. Engng* **50** (2001) 2031–2051.

11. M. P. Bendsøe, *Optimization of Structural Topology, Shape and Material* (Springer, Berlin 1995).

12. K. Lurie, *Applied Optimal Control Theory of Distributed Systems* (Plenum Press, New York 1993).

13. A. Cherkaev and R. V. Kohn, *Topics in the Mathematical Modelling of Composite Materials* (Birkhäuser, Boston 1997).

14. A. Cherkaev, *Variational Methods for Structural Optimization* (Springer, New York 2000).

15. T. Lewinski and J. J. Telega, *Plates, Laminates and Shells. Asymptotic Analysis and Homogenization* (World Scientific, Singapore 2000).

16. L. Tartar, An introduction to the homogenization method in optimal design, *Optimal Shape Design*, Lecture Notes in Mathematics 1740 (eds A. Cellina and A. Ornelas; Springer, Berlin 2000) 47–156.

17. G. Allaire, *Shape Optimization by the Homogenization Method* (Springer, New York 2002).

18. M. P. Bendsøe and O. Sigmund, *Topology Optimization, Theory, Methods and Applications* (Springer, Berlin 2003).

19. A. J. Markworth, K. S. Ramesh and W. P. Parks, Modelling studies applied to functionally graded materials, *J. Materials Sci.* **30** (1995) 2183–2193.

20. Y. Ootao, Y. Tanigawa and O. Ishimaru, Optimization of material composition of functionally graded plate for thermal stress relaxation using a genetic algorithm, *J. Thermal Stresses* **23** (2000) 257–271.

21. P. Duysinx and M. P. Bendsoe, Topology optimization of continuum structures with local stress constraints, *Int. J. Numer. Meth. Engng* **43** (1998) 1453-1478.

22. R. Lipton, Design of functionally graded composite structures in the presence of stress constraints, *Int. J. Sol. Str.* **39** (2002) 2575–2586.

23. R. Lipton, Homogenization and design of functionally graded composites for stiffness and strength, *Nonlinear Homogenization and its Application to Composites, Polycrystals, and Smart Materials* (eds P. Ponte Castaneda and J. J. Telega; Springer, Berlin 2004) 169–192.

24. G. Allaire, F. Jouve and H. Mallot, Topology optimization for minimum stress design with the homogenization method, *Struct. Multidisc. Optim.* **28** (2004) 87–98.

25. L. Tartar, Remarks on optimal design problems, *Calculus of Variations, Homogenization and Continuum Mechanics* (eds G. Buttazzo, G. Bouchitte and P. Suquet; World Scientific, Singapore 1994) 279–296.

26. A. Velo, Optimal design of gradient fields with applications to electrostatics, Ph.D. Thesis, Department of Mathematical Sciences, Worcester Polytechnic Institute (2000).

27. R. Lipton and A. Velo, Optimal design of gradient fields with applications to electrostatics, *Nonlinear Partial Differential Equations and Their Applications: College de France Seminar* Vol. XIV, *Studies in Mathematics and its Applications* (North–Holland, Elsevier, Amsterdam 2002) 509–532.

28. Y. Grabovsky, Optimal design problems for two-phase conducting composites with weakly discontinuous objective functionals, *Adv. Appl. Maths.* **27** (2001) 683–704.

29. P. Pedregal, Fully explicit quasiconvexification of the square of the gradient of the state in optimal design, *Electronic Research Announcements of the Amer. Math. Soc.* **7** (2001) 72–78.

30. K. A. Lurie, The extension of optimization problems containing controls in the coefficients, *Proc. R. Soc. Edinburgh* A **114** (1990) 81–97.

31. R. Lipton, Assessment of the local stress state through macroscopic variables, *Phil. Trans. R. Soc.* A **361** (2003) 921–946.

32. R. Lipton, Bounds on the distribution of extreme values for the stress in composite materials, *J. Mech. Phys. Solids* **52** (2004) 1053–1069.

33. R. Lipton, Homogenization theory and the assessment of extreme field values in composites with random microstructure, *SIAM J. Appl. Math.* **65** (2004) 475–493.

34. B. Bourdin, Filters in topology optimization, *Int. J. Numer. Meth. Engng* **50** (2001) 2143–2158.

35. S. Spagnolo, Convergence in energy for elliptic operators, *Proc. Third Symp. on Numerical Solutions of Partial Differential Equations* (ed. B. Hubbard; Academic Press, New York 1976) 469–498.

36. F. Murat and L. Tartar, H-convergence, *Séminaire d'Analyse Fonctionnelle et Numérique de l'Université d'Alger.* Mimeographed notes: 1978. English translation: *Topics in the Mathematical Modeling of Composite Materials* (eds A. Cherkaev and R. V. Kohn; Birkhäuser, Boston 1997) 21–43.

37. L. C. Evans, *Weak Convergence Methods for Nonlinear Partial Differential Equations* (American Mathematical Society, Providence 1990).

38. V. V. Jikov, S. M. Kozlov and O. A. Oleinik, *Homogenization of Differential Operators and Integral Functionals* (Springer, Berlin 1994).

39. M. Briane, Correctors for the homogenization of a laminate, *Advances in Mathematical Sciences and Applications* 4, (Gakkotosho, Tokyo, 1994) 357–379.